Surface x-ray-scattering measurements of the substrate-induced spatial modulation of an incommensurate adsorbed monolayer

Michael F. Toney, Joseph G. Gordon, Mahesh G. Samant, Gary L. Borges, Owen R. Melroy, Lung-Shan Kau, and David G. Wiesler
IBM Almaden Research Center, IBM Research Division, San Jose, California 95120

Dennis Yee and Larry B. Sorensen
Department of Physics, FM-15, University of Washington, Seattle, Washington 98195
(Received 20 February 1990; revised manuscript received 27 April 1990)

We report *in situ* surface x-ray-scattering measurements of electrochemically deposited Tl monolayers on Ag(111). We find that the Tl adlayer forms an incommensurate, two-dimensional solid, and we determine the spatial modulation in the Tl monolayer that is induced by the periodic potential of the substrate. The modulation of the Tl monolayer changes the intensity of the x-ray scattering from the Ag substrate (the Ag crystal truncation rods), since the modulation wave vectors are commensurate with the substrate periodicity. By measuring the intensity changes along the Ag truncation rods, we determined the first Fourier component of the longitudinal part of the substrate-induced modulation to be 0.03 Å, and the spacing of the Tl monolayer above the Ag surface to be 3.05 Å. In addition, from the phase of the monolayer scattering amplitude (relative to the substrate scattering amplitude) required to fit the data, the lowest-energy sites on the surface are identified as the threefold-hollow sites. Using the Novaco-McTague model and estimates of the elastic susceptibility of the Tl monolayer, we also estimate the first Fourier component of the surface energy corrugation to be 2–3 meV (0.05–0.07 kcal/mol). To obtain the modulation amplitude, we have analyzed the ratio of the Ag truncation-rod intensities with and without the monolayer rather than the intensities. The use of the "ratio" method was very important because the ratio is considerably more accurate than the intensities. We also find that the bare Ag(111) surface in contact with electrolyte is very flat (a rms roughness of 0.7 Å) compared with similar metal surfaces prepared by sputtering and annealing in vacuum (rms roughness ~3–5 Å).

I. INTRODUCTION

The periodic potential of a substrate has important influences on the crystallographic structure, lattice constants, and orientation of thin films that are grown on it. When the adsorbate-substrate interactions are much stronger than the adsorbate-adsorbate interactions (i.e., the strong-substrate limit), the substrate periodicity dictates the structure of the thin adsorbed film. This results in the formation of a commensurate or registered film, and under suitable conditions, pseudomorphic growth. If the adsorbate-substrate interactions are much weaker than the adsorbate-adsorbate interactions (i.e., the weak-substrate limit), then the thin film assumes an incommensurate structure that is much closer to the crystallographic structure it would have if the substrate were absent. However, the substrate still has some influence, since its periodic potential creates small amplitude, static displacements in the atomic positions of the thin adsorbed layer.[1,2] This static distortion wave (or substrate-induced spatial modulation) can lead to a rotation of the adsorbed layer with respect to the substrate, as predicted by Novaco and McTague (NM),[3,4] and to commensurate-incommensurate phase transitions.[5] Because the substrate-induced modulation has Fourier components (i.e., wave vectors) that are commensurate with the substrate periodicity, the scattering from the *modulated incommensurate* adsorbed layer interferes coherently with scattering from the substrate. Thus the adsorption of the thin film changes the apparent intensity of the substrate diffraction. These changes can be used to determine the amplitude of the modulation, the separation between the substrate and adlayer, and the lowest-energy positions on the surface.

We have observed this interference by measuring the surface x-ray scattering (crystal truncation rods) from Ag(111) substrates with and without a monolayer of Tl. The Tl is deposited (and removed) electrochemically and forms an ordered, incommensurate, hexagonal monolayer. The measurements were conducted *in situ* (in contact with the electrolyte) and under potential control. From the ratio of the truncation-rod intensities with and without the monolayer, we have determined that the longitudinal part of the first Fourier component of the substrate-induced modulation is 0.031±0.005 Å and that the average spacing of the Tl monolayer above the Ag surface is 3.05±0.1 Å. In addition, the phase of the monolayer scattering amplitude was determined and shows that the lowest-energy positions on the surface are the threefold-hollow sites. The use of the intensity ratio was very important, because the geometrical scattering corrections cancel out of the ratio, and hence, the ratio is

more accurate than the corrected intensities. By using the NM model[3,4] and estimates of the elastic susceptibility of the Tl monolayer, we also estimate the first Fourier component of the surface energy corrugation to be 2–3 meV (0.05–0.07 kcal/mol).

The remainder of the paper is organized as follows. In Sec. II we first discuss substrate-induced spatial modulation of adlayers and then calculate how this modifies the scattering intensity at the substrate diffraction wave vectors. In Sec. III the experimental details are outlined. The electrochemical deposition of Tl on Ag(111), the surface scattering data (including the necessary experimental corrections), and the data analysis are discussed in Sec. IV. In Section V our estimate of the surface potential energy corrugation is described, and our results are discussed and compared with other measurements.[6,9] The final section contains concluding remarks.

II. SUBSTRATE-INDUCED SPATIAL MODULATION OF ADLAYERS

Figure 1 illustrates, in a one-dimensional model, the origin of the substrate-induced spatial modulation in an adsorbed monolayer.[1,2] Although the adlayer is incommensurate with the substrate, its energy is reduced when the local positions of the adatoms shift slightly as they tend to move toward positions of lower energy. These shifts are the substrate-induced spatial modulation $\mathbf{u}_j$ and they have the same in-plane periodicity as the substrate. Thus, denoting the position of the jth adatom in the absence of the substrate as $\mathbf{R}_j$, the modulation can be expanded in terms of the in-plane substrate wave vectors.

$$\mathbf{u}_j = \sum_{\mathbf{G}} \mathbf{u}_{\mathbf{G}} \exp(i\mathbf{G}\cdot\mathbf{R}_j) , \tag{1}$$

where $\mathbf{G}$ is a reciprocal-lattice vector of the substrate surface (in the plane of the surface) and $\mathbf{u}_{\mathbf{G}}$ is the amplitude of the modulation with wave vector $\mathbf{G}$.[3,4,10] The magnitude of $\mathbf{u}_{\mathbf{G}}$ is determined by the lattice mismatch between the adsorbate and substrate and by the ratio of the adsorbate-adsorbate to adsorbate-substrate interaction potentials. The modulation will be small if the adatom-substrate potential is weak compared to the adatom-adatom potential and the adlayer lattice spacing does not closely match the substrate lattice. If the opposite is true, $\mathbf{u}_{\mathbf{G}}$ will be large.

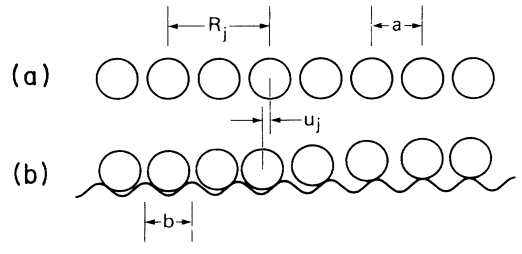

FIG. 1. One-dimensional, schematic illustration of the spatial modulation induced by the substrate potential. (a) Unmodulated adlayer in the absence of a substrate. The adatom positions are $\mathbf{R}_j$. (b) Modulated adlayer. The adatom positions have shifted to $\mathbf{R}_j+\mathbf{u}_j$ due to the substrate potential. The unmodulated spacing between atoms in the adlayer and substrate are a and b, respectively.

We have made the assumption in Eq. (1) that the modulation $\mathbf{u}_j$ is small, and hence, the adlayer response to the substrate potential is linear. Our results demonstrate that this approximation is valid. We also assume, as usual,[3,4,10] that the modulation normal to the surface is negligibly small. In addition, we assume that only the lowest-order set of symmetry equivalent $\{\mathbf{G}\}$ contributes to the sum in Eq. (1), since the amplitudes $\mathbf{u}_{\mathbf{G}}$ with these wave vectors are small and higher-order harmonics are likely smaller. For convenience, we choose the real-space origin to be the site of a substrate atom in the top layer, so that the modulation is centrosymmetric ($\mathbf{u}_j=-\mathbf{u}_{-j}$) and $\mathbf{u}_{\mathbf{G}}$ is purely imaginary.

The scattering amplitude $A_m(\mathbf{Q})$ for the modulated incommensurate layer at scattering vector $\mathbf{Q}$ is

$$\begin{aligned} A_m(\mathbf{Q}) &= F_m(\mathbf{Q}) \sum_j \exp[-i\mathbf{Q}\cdot(\mathbf{R}_j+\mathbf{u}_j)] \\ &\simeq F_m(\mathbf{Q}) \sum_j (1-i\mathbf{Q}\cdot\mathbf{u}_j)\exp(-i\mathbf{Q}\cdot\mathbf{R}_j) , \end{aligned} \tag{2}$$

where F_m is the atomic scattering factor of the adatoms and we have again assumed the modulation is small. Substituting the expression for the modulation $\mathbf{u}_j$ [Eq. (1)] into Eq. (2) yields

$$\begin{aligned} A_m(\mathbf{Q}) = N_m F_m(\mathbf{Q}) \Big[&\sum_{\tau} \delta(\mathbf{Q}_\parallel - \tau) \\ &- i \sum_{\tau} \sum_{\mathbf{G}} \mathbf{Q}\cdot\mathbf{u}_{\mathbf{G}} \delta(\mathbf{Q}_\parallel - (\mathbf{G}-\tau)) \Big] , \end{aligned} \tag{3}$$

where δ is the Dirac δ function, τ is an in-plane reciprocal-lattice vector of the unmodulated incommensurate adlayer, $\mathbf{Q}_\parallel$ is the component of $\mathbf{Q}$ parallel to the surface, and N_m is the total number of atoms in the adlayer. The leading term represents the main diffraction peaks at the adlayer reciprocal-lattice vectors. The second term represents the "modulation superlattice" diffraction peaks (also known as "satellite" peaks), which are found at $\mathbf{Q}_\parallel=\{\mathbf{G}\}-\{\tau\}$. These have been observed for strongly modulated adlayers, such as Kr on graphite;[9] analogous satellite peaks have been observed in three-dimensional (3D) materials when the atomic positions are modulated with a periodicity that is incommensurate with the 3D lattice.[11–13] In this paper we concentrate on the adlayer scattering with $\tau=\mathbf{0}$, which occurs at the substrate-surface reciprocal-lattice vectors $\mathbf{Q}_\parallel=\mathbf{G}$, and hence, interferes with the scattering from the substrate. Because the scattering amplitude from a monolayer is only of order N_m the interference is only important when the substrate scattering amplitude is of the same order; this occurs near the antinodes of the substrate crystal truncation rods.

The termination of a crystal at a surface or interface gives rise to tails of scattering intensity about bulk Bragg peaks extending along a direction normal to the surface.[14–17] Taking the z direction as the surface normal,

this scattering occurs along rods with $\mathbf{Q}=\mathbf{G}+Q_z\hat{\mathbf{z}}$, where Q_z is the component of the scattering vector in the z direction. These rods of scattering have been termed crystal truncation rods (CTR's).[14] The CTR scattering amplitude for a perfectly flat (111) face-centered-cubic (fcc) crystal is[14,18]

$$A_s(\mathbf{Q})=\frac{N_sF_s(\mathbf{Q})}{1-\exp(iK)}\ , \tag{4}$$

where $K=(2\pi/3)(h-k)+CQ_z$, C is the layer spacing, N_s is the number of atoms in a single (111) layer of the substrate, and F_s is the atomic scattering factor of the substrate atoms. We have adopted a hexagonal unit cell (denoted h) for the fcc crystal with

$$\begin{aligned}&(100)_h=\tfrac{1}{3}(4\,\bar{2}\,\bar{2})_c,\quad (010)_h=\tfrac{1}{3}(22\bar{4})_c,\\&(001)_h=\tfrac{1}{3}(111)_c\ ,\end{aligned} \tag{5}$$

where c refers to the cubic unit cell.

The total CTR scattering amplitude, $A(\mathbf{Q})$, for a modulated, incommensurate adlayer adsorbed on an undistorted substrate is the sum of the amplitudes from the bare substrate and the adlayer:[19]

$$\begin{aligned}A(\mathbf{Q})&=A_s+A_m\\&=\frac{N_sF_s(\mathbf{Q})}{1-\exp(iK)}-iN_mF_m(\mathbf{Q})(\mathbf{G}\cdot\mathbf{u}_\mathbf{G})\exp(-idQ_z)\ ,\end{aligned} \tag{6}$$

where d is the average (center-to-center) spacing of the monolayer above the top layer of the substrate. Because $\mathbf{u}_\mathbf{G}$ is imaginary, the phase of the adlayer scattering (the phase of the second term) is either 0 or π when $Q_z=0$ [i.e., $i(\mathbf{G}\cdot\mathbf{u}_\mathbf{G})$ can be either positive or negative]. Since the interference between the adlayer and the substrate scattering amplitudes changes the CTR scattering, measurements of the CTR intensity can be used to determine the longitudinal (i.e., along $\mathbf{G}$) Fourier components of the modulation ($\mathbf{G}\cdot\mathbf{u}_\mathbf{G}$) and the substrate-monolayer separation d.

Until now, we have implicitly assumed that the substrate surface is perfectly flat. Of course, real surfaces are not perfectly flat but have atomic scale roughness (e.g., steps). This roughness can be included in our analysis in a convenient way by using the simple, real-space model introduced by Robinson.[14] In this model, partially filled layers are added to the surface and each added layer has a fractional occupancy β ($0<\beta<1$) relative to the layer below. This model can account for stepped surfaces and with it the CTR intensity $I=|A|^2$ becomes

$$I=\frac{(1-\beta)^2}{1+\beta^2-2\beta\cos K}\left|\frac{N_sF_s(\mathbf{Q})}{1-\exp(iK)}-iN_mF_m(\mathbf{Q})(\mathbf{G}\cdot\mathbf{u}_\mathbf{G})\times\exp(-idQ_z)\right|^2. \tag{7}$$

Here $\beta=0$ represents a perfectly flat surface, while $\beta=1$ is infinitely rough. It is perhaps more physical to think of the surface roughness in terms of the root-mean-square (rms) roughness, which in this fractional-occupancy model is given by $[\sqrt{\beta}/(1-\beta)]C$,[14] where C is the layer spacing.

The fractional-occupancy model is only one of several that can describe an imperfect surface. For example, CTR data have been fitted successfully with models that do not have rough (e.g., stepped) surfaces but instead have enhanced disorder in the topmost substrate layer.[15,20] In these models the disorder was parametrized with an enhanced Debye-Waller factor. Since these models fit our data as well as the fractional-occupancy model, we cannot distinguish between the various models. We use the fractional-occupancy model solely for convenience.

III. EXPERIMENT

All of our experiments were performed *in situ* (in electrolyte), under potential control, and at room temperature. The electrochemical cell is essentially the same as that used to investigate electrochemically deposited Pb on Ag(111) and Au(111) and has been described in detail.[21,22] To prevent oxidation of the monolayer caused by diffusion of atmospheric O_2 through the polypropylene film that confines the electrolyte, we flow Ar gas through a cylindrical Kapton window that surrounds the polypropylene film and the electrode. With this arrangement, no changes in the diffraction pattern from the monolayer were observed over a period of one day. The electrode substrates were epitaxially grown thin films of Ag that were vapor deposited onto freshly cleaved mica.[21,22] The electrolyte was 0.1 M Na_2SO_4 containing 2.5 mM Tl_2SO_4. The Tl monolayer was deposited with the cell inflated so a relatively thick ($\sim$ 1 mm) layer of electrolyte covers the electrode. The electrolyte was then partially withdrawn and the diffraction data were measured through a thin ($\lesssim 30$ μm) layer of electrolyte. All potentials are reported relative to the Ag/AgCl (3 M KCl) reference electrode.

The data were collected at the National Synchrotron Light Source (NSLS) beam line X20A.[23] An incident x-ray energy of 9997 eV (1.240 Å) was selected using a Si(111) double monochromator. At the sample the focused x-ray beam had a vertical and horizontal full width at half maximum (FWHM) of 0.8 and 1.7 mm, respectively. The incident beam intensity was monitored by a NaI scintillation detector viewing a Kapton beam splitter. The diffracted beam was analyzed with 1 mrad Soller slits and the intensity was measured with a NaI scintillation detector. The sample was aligned using the bulk Ag $(101)_h$ and $(011)_h$ reflections; all data were obtained in the symmetric ($\omega=0$) mode.[24]

IV. RESULTS

Before describing our x-ray measurements, we first discuss the underpotential electrochemical deposition of Tl on Ag(111). Electrochemical deposition of metal layers onto a foreign metal substrate frequently occurs in distinct stages with the initial formation of one (or more) layers at electrode potentials positive of the reversible thermodynamic (Nernst) potential for bulk deposition.[25,26] This process is thus termed underpotential deposition (UPD). On single crystals, these initial depos-

its are believed to be well-defined, ordered layers.[27] The UPD layers are frequently deposited by linearly sweeping the electrode potential in the negative direction from a suitable positive potential. Figure 2 shows a typical current response of the Ag electrode to a linear potential sweep (a cyclic voltammogram) for Tl on Ag(111).[28,29] If the adsorbing ion is completely discharged [as for Tl/Ag(111) (Ref. 28)] and kinetic effects are absent, the current response is proportional to the derivative of the adsorption isotherm.[30]

The predominant features in Fig. 2 are two large, sharp peaks. The first, at approximately −470 mV (240 mV positive of the Nernst potential) has previously been attributed to the deposition of a monolayer of Tl.[28,30,31] Figure 3(a) shows the in-plane diffraction pattern (at $Q_z=0$) for this layer determined from our *in situ* x-ray-scattering data. Examples of a radial and azimuthal scan of a first-order Bragg rod from the Tl monolayer are shown in Figs. 3(b) and 3(c), respectively. The diffraction pattern together with out-of-plane scans of the Bragg rods[32] show that this Tl layer is a two-dimensional (2D), incommensurate hexagonal monolayer that is slightly compressed from the bulk metal and rotated about 4°–5° from the Ag $[100]_h$ direction. These results together with the potential dependence of the monolayer structure will be reported in detail elsewhere.[32] The second peak in Fig. 2 corresponds to the deposition of a second layer of Tl on top of the first, forming a bilayer where the two layers are mutually commensurate. Like the Tl monolayer, the bilayer is incommensurate with the Ag substrate and has a hexagonal structure that is slightly compressed relative to bulk Tl (although it is less compressed than the monolayer) and is rotated about 4° from the Ag $[100]_h$ direction.[32]

Figures 4(a) and 4(b) show, respectively, the intensities of the Ag $(1,0,Q_z)_h$ rods with and without the Tl monolayer present. These data were obtained by measuring the peak intensity and subtracting the background (which was obtained at an azimuthal angle 1° from the peak). Since azimuthal scans at several different Q_z showed that

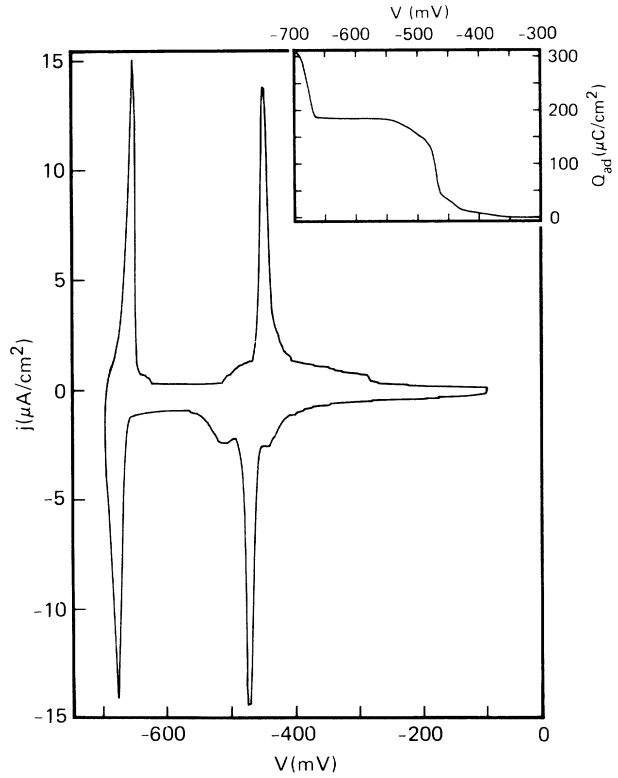

FIG. 2. Cyclic voltammogram (current-vs-voltage scan) for the deposition of Tl on Ag(111) in 2.5×10^{-3} M Tl_2SO_4 and 0.1 M Na_2SO_4. The potentials were measured relative to Ag/AgCl and the scan rate was 2 mV/sec. The first large peak (at approximately −470 mV) corresponds to the deposition of a single monolayer of Tl, while the second peak corresponds to the deposition of a second layer (bilayer). The Nernst potential for bulk deposition is −710 mV. The inset shows the adsorption isotherm, which is the integral of the cyclic voltammogram or the charge, Q_{ad}, that flows into the electrode during Tl deposition. There is a background current due to processes that do not involve deposition of Tl. A linear current (passing through the cyclic voltammogram at $V=-600$ and −180 mV) was used to estimate this background and has been subtracted from the data in the calculation of Q_{ad}.

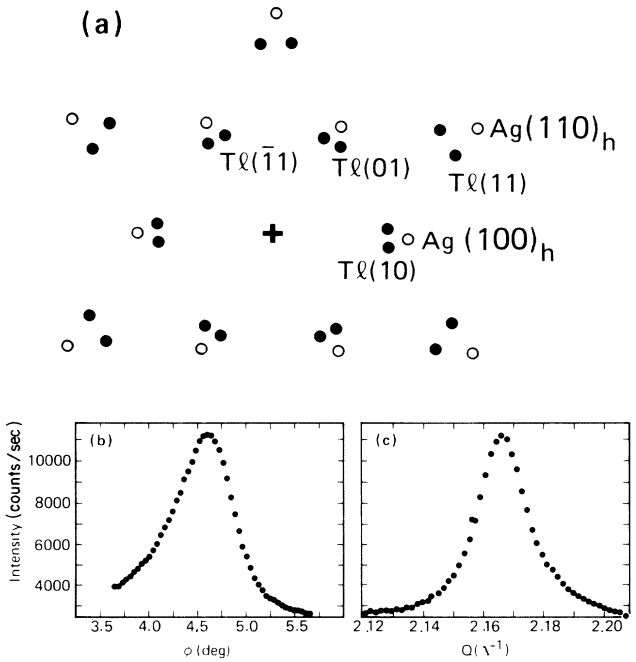

FIG. 3. X-ray diffraction from Tl on Ag(111). (a) In-plane diffraction pattern ($Q_z=0$) for a monolayer of Tl. The center of the pattern is illustrated with a plus, the Ag reflections with open circles, and the Tl reflections with solid circles. There are two observed domains, oriented ±4°–5° from the Ag $(100)_h$ direction. (b) An azimuthal angle scan of the Tl (10) Bragg rod at fixed $Q=2.165$ Å^{-1}. The angle ϕ is the angle between **Q** and the Ag $(100)_h$ direction, and the scan was made at a deposition potential of −550 mV. (c) A radial scan of the Tl (10) Bragg rod. In this scan the magnitude of the scattering vector $Q=|\mathbf{Q}|$ was varied and was fixed at 4.6°. These data, together with out-of-plane scans of the Tl Bragg rods (Ref. 32) show that the Tl deposit is an incommensurate hexagonal monolayer.

the azimuthal width did not depend on Q_z, or on the presence or absence of Tl, we have used the peak intensity (rather than the azimuthally integrated intensities) in the data analysis. To compare the data with the calculated CTR intensity [Eq. (7)], the data must be corrected for the active sample area, Lorentz factor, Ag scattering factor, and resolution function. The sample area and resolution function corrections will be described in detail elsewhere.[32]

Briefly, the resolution function correction accounts for the overlap between the surface scattering and the highly anisotropic resolution volume associated with our scattering geometry.[33,34] The anisotropic resolution volume tilts as a scan is made along the CTR, resulting in a decreasing overlap with increasing Q_z. To correct the experimental data for this, the shape of the resolution volume must be known. We have made careful scans at several points along the CTR and fit these to a resolution volume that has a broad "slitlike" shape in the out-of-plane direction (FWHM of 0.12 Å^{-1}) and a sharper shape in the in-plane direction.[32] When convolved with the finite size of the Ag surface domains, the in-plane peak shapes are described by a Lorentzian squared form (FWHM of 0.016 Å^{-1}),[32] although we do not attach any physical significance to this form and have used it only for convenience. The experimental data are corrected using the measured, anisotropic reciprocal-space volume (i.e., a 0.12 Å^{-1} "slitlike" out-of-plane shape and a 0.016 Å^{-1} Lorentzian-squared in-plane shape). The sample area correction compensates for the variable illumination of the sample with incidence angle α; at small α all of the sample is illuminated, while at larger α only a portion (inversely proportional to $\sin\alpha$) is illuminated. This correction is made using the measured beam shape. We estimate that when the experimental data have been corrected for sample area, Lorentz factor, Ag scattering factor, and resolution function they are accurate to about 5%. This uncertainty is due to inaccurate knowledge of the area and resolution function corrections.[32]

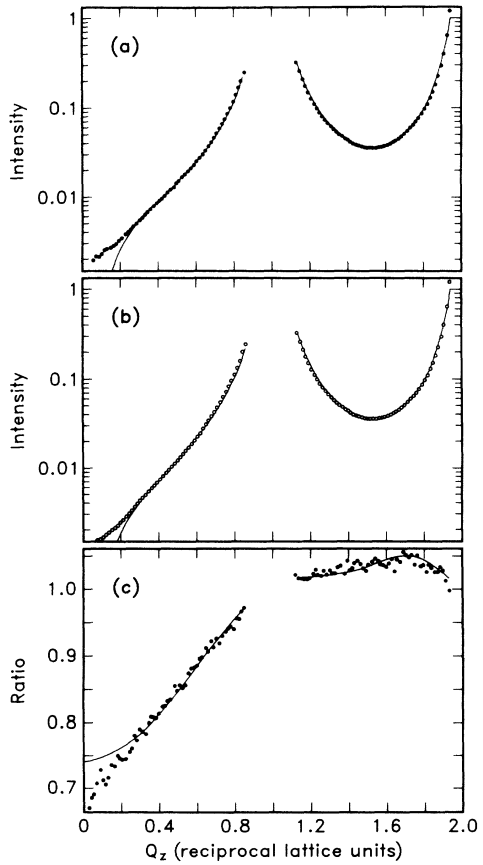

FIG. 4. Intensity of the Ag $(1,0,Q_z)_h$ crystal truncation rod. (a) Bare Ag surface at $V=-200$ mV. The data are shown by the solid circles and the best fit by the solid line. (b) Tl monolayer on Ag at $V=-600$ mV. The data are shown by the open circles and the best fit by the solid line. (c) The ratio of the CTR intensity with the Tl monolayer present, (b), to the CTR intensity with the monolayer absent, (a). The data sets shown in (a) and (b) are both averages of eight separate CTR scans and have a reproducibility of about 1%.

The data from the Ag substrate without the Tl monolayer were fit to the CTR intensity of a bare substrate with some roughness. The CTR intensity was modeled using Eq. (7) with $N_m=0$ (i.e., bare) and four fitting parameters: (1) the roughness factor β, (2) an overall scale factor, (3) the x-ray adsorption due to the electrolyte and polypropylene film covering the Ag electrode, and (4) the fraction of *CBA* (relative to *ABC*) stacking in the Ag substrate. The last parameter is necessary because the vapor-deposited Ag thin films used in this work have both *ABC* and *CBA* stacking. Consequently, the rod scans shown in Fig. 4 contain contributions from both the $(1,0,Q_z)_h$ and the $(0,1,Q_z)_h$ Ag CTR's. Since these contributions are not equal, the relative fractions of each stacking sequence must also be fit to the data. For the data shown in Fig. 4, the best fit gives 0.62 *ABC* and 0.38 *CBA*. This fraction was checked by measurements of the intensities of the $(102)_h$ and $(011)_h$ bulk Bragg peaks relative to the bulk Bragg peaks rotated 60° from these; we found that this gave consistent *ABC*/*CBA* stacking fractions. Similar fractions are found for several other Ag films.[35]

The x-ray absorption by the material covering the electrode reduces the observed intensity by $\exp[-(2\mu t/\sin\alpha)]$, where α is the incidence angle and $2\mu t$ is the absorption of the incident and diffracted x rays by the polypropylene film and the electrolyte. In these experiments, the angular acceptance of the scattered x rays in the out-of-plane direction was (purposely) rather large ($\simeq 1.4°$), which results in a fairly large spread in exit angles. Thus, the absorption correction must be integrated over this range of exit angles. This effect was taken into account when fitting the data, but is only important at small Q_z. Since the thickness (6.3 μm) and composition of the polypropylene film are known, and the composition of the electrolyte is also known, we can estimate the electrolyte thickness from the value of μt. The best fit value is $\mu t=0.016$, which yields an average electrolyte thickness of 30 μm.

The best fit to the CTR intensity for the bare Ag substrate is shown by the solid line in Fig. 4(a). The fit is quite good for most Q_z. However, it is not very good at small Q_z ($\lesssim 0.3$), which is probably caused by nonunifor-

mities in the thickness of the electrolyte layer. The absorption correction is highly nonlinear at small Q_z [since it is an exponential of (electrolyte thickness)/Q_z]. Thus, regions of the sample with an electrolyte thickness that is slightly smaller than average will disproportionately contribute to the measured intensity at small Q_z. This effect is not accounted for with the simple correction given here, since the electrolyte thickness is assumed to be uniform. At larger Q_z, the effect of nonuniformities becomes much smaller, since the correction becomes much more linear. Consequently, the data were only fit for $Q_z > 0.3$.

The best fit to the data for the bare Ag surface yields a value of $\beta = 0.08 \pm 0.02$ or a rms roughness of 0.7 ± 0.1 Å. This demonstrates that the Ag substrates under potential control and in contact with an electrolyte are very smooth. Indeed, this surface is much smoother than metal surfaces prepared by sputtering and annealing in a vacuum environment, which have roughness parameters $\beta \sim 0.5$–0.7, or rms roughness of 3–5 Å.[14,20] This suggests that the Ag(111) surface is inherently smooth in an aqueous environment at this potential (−200 mV, well negative of the dissolution potential for Ag).

Figure 4(c) shows the ratio of the CTR intensity with the Tl monolayer present ($V = -600$ mV) to that with the monolayer ($V = -200$ mV) absent. By taking this ratio, the instrumental corrections and the solution absorption correction cancel; thus, the uncertainty in the ratio is considerably smaller than the uncertainties in the corrected intensities. The ratio clearly shows that when the monolayer is adsorbed the CTR intensity is decreased for $Q_z \lesssim 1$, but increased slightly for $1 \lesssim Q_z \lesssim 2$. This change cannot be explained simply by an increase in surface roughness, since this would decrease the CTR intensity at all Q_z. However, the change is consistent with the interference expected for the adsorption of a spatially modulated incommensurate monolayer on the Ag substrate. This monolayer-present ($N_m \neq 0$) to monolayer-absent ($N_m = 0$) ratio is calculated using the expression for CTR intensities [Eq. (7)]:

$$R = \left| 1 - i \frac{[1 - \exp(iK)] N_m F_m(\mathbf{Q}) (\mathbf{G} \cdot \mathbf{u}_G) \exp(-id Q_z)}{N_s F_s(\mathbf{Q})} \right|^2 , \tag{8}$$

where $\mathbf{G}$ is the Ag $(100)_h$ reciprocal-lattice vector.

The best fit of the observed CTR intensity ratio to Eq. (8) is shown by the solid line in Fig. 4(c). The fit is excellent over most of the data range. The slight deviation from the data for $0 \lesssim Q_z \lesssim 0.15$ is probably caused by very small changes in the nonuniformities in solution thickness as discussed above. Only two parameters were used in this fit: the Ag-Tl spacing d and the first longitudinal Fourier component of the modulation, $u_G^l \equiv i(\mathbf{u}_G \cdot \mathbf{G})/|\mathbf{G}|$ for $\mathbf{G} = (100)_h$.[48] The overall scale factor, electrolyte absorption, and roughness β were all assumed to be the same as the bare substrate and are thus canceled out by taking the ratio. In addition, we use the *ABC/CBA* stacking fractions determined from the fit for the bare Ag substrate. The line in Fig. 4(b) shows the corresponding CTR intensity with the Tl monolayer present; this is calculated using these same values of β, scale factor, electrolyte absorption, *CBA* stacking fraction, and the best-fit values of u_G^l [$\mathbf{G} = (100)_h$] and d. The agreement between the calculated CTR intensity and the data is very good and is comparable to that in Fig. 4(a).

From the fit, the first Fourier component of the substrate-induced modulation in the incommensurate Tl monolayer is determined to be u_G^l [$\mathbf{G} = (100)_h$] $= +0.031 \pm 0.005$ Å. This is a very small modulation compared to the 3.34 Å near-neighbor spacing of the Tl monolayer[32] and confirms our initial assumption that the modulation is small enough so the adlayer responds linearly to the substrate potential. An adequate fit can be obtained only if the relative phase between the substrate and monolayer scattering is 0, which requires u_G^l to be positive. Since the real-space origin is chosen as a Ag atom in the top layer, this shows that the adatoms prefer to move away from the on-top sites and toward threefold-hollow sites. When the unmodulated position $\mathbf{R}_j$ is close to an on-top site ($\mathbf{G} \cdot \mathbf{R}_j \simeq 2n\pi$, n an integer), the exponential in the expression for the modulation $\mathbf{u}_j$ [Eq. (1)] can be approximated as $\exp(i\mathbf{G} \cdot \mathbf{R}_j) = 1 + i(\mathbf{G} \cdot \mathbf{R}_j - 2n\pi)$. From Eq. (1) together with symmetry ($\mathbf{u}_j$ is real and centrosymmetric, so $\mathbf{u}_G$ is imaginary and centrosymmetric), one can show that the adatoms tend to shift away from the on-top sites. An analogous argument for $\mathbf{R}_j$ close to the threefold-hollow sites [$\mathbf{G} \cdot \mathbf{R}_j \simeq (2n+1)\pi \pm \pi/3$] shows that the adatoms tend to move toward these sites. As discussed below, this preferred motion is reasonable, since the potential-energy minima are the threefold-hollow sites.

The best-fit value for the average spacing between the Tl monolayer and the Ag substrate is 3.05 ± 0.1 Å. For an incommensurate adlayer it is not immediately obvious that one can determine this spacing by measuring the off-specular ($Q_\parallel \neq 0$) scattering from the substrate (or even that an *incommensurate* adlayer will change the off-specular scattering from the *substrate* at all). However, the substrate-induced spatial modulation in the adlayer makes this measurement possible, since the modulation wave vectors are commensurate with the substrate periodicity.

The CTR intensities with and without the Tl monolayer were also measured on a different Ag substrate than that used for the data shown in Fig. 4. Although the uncertainties in this data set are larger than in the data set shown in Fig. 4, they were also analyzed as described above. The results for the modulation, the Tl-Ag spacing, and the surface roughness are, respectively, $u_G^l = 0.034$ Å, $d = 3.15$ Å, and $\beta = 0.10$ (a rms roughness of 0.8 Å). These values are all within estimated errors quoted above, which gives us confidence that our results are correct. The solution thickness is slightly smaller, 20 μm compared to 30 μm. This is likely due to a different azimuthal orientation of the clip that retains the substrate or a slightly different tension on the polypropylene film covering the electrode.[21,22]

V. DISCUSSION

We have determined the substrate-induced modulation of an incommensurate Tl monolayer, by measuring the

ratio of the Ag $(100)_h$ CTR with and without the monolayer adsorbed. It is important to note that in this "ratio method" all the instrumental corrections cancel out exactly, and for a given Ag substrate, the solution absorption correction also cancels. Thus, there is no uncertainty in the ratio due to inaccurate knowledge of the sample area correction or the resolution function correction. We estimate that the accuracy of the ratio is about 1.5%, based on the reproducibility of these data. This is limited primarily by counting statistics and small displacements of the Ag substrate and the polypropylene film that occur when electrolyte is added and removed from the cell during adlayer deposition and stripping. This accuracy is considerably better than the estimated 5% error in the corrected intensities. The ratio method is, thus, extremely effective and was essential for these measurements.

Although we are able to fit the data in Fig. 4 quite well with a CTR intensity due to a substrate-modulated incommensurate adlayer, other explanations are possible. As mentioned above, the decrease in CTR intensity at small Q_z and the increase at large Q_z cannot be explained by a change in surface roughness (either with different β or with enhanced disorder in the top substrate layer). A model with large changes in the interlayer spacings between the top three Ag layers (relaxation of these layers) can fit the data. However, the required changes are much too large (0.1–0.2 Å) to be physically reasonable. For (111) surfaces of fcc crystals, the first layer relaxation is generally $\lesssim 0.02$ Å and deeper layers do not relax.[36] We have also checked the assumption that the surface roughness (described by β) does not change when the Tl monolayer is adsorbed. The fit to the ratio in Fig. 4(c) is not improved if β is allowed to vary as a fitting parameter. This demonstrates that the substrate does not become significantly rougher when the UPD monolayer is adsorbed.

The substrate-induced spatial modulation is directly related to the elastic susceptibility of the incommensurate adlayer and to the substrate potential-energy corrugation; if the adlayer is soft and the energy corrugation is large, then the modulation will be large. This argument is qualitative. We can obtain a semiquantitative estimate of the substrate corrugation by using the model developed by Novaco and McTague (NM),[3,4] together with an estimate of the elastic susceptibility of the adlayer. NM calculate the energy change of the adlayer due to the creation of a periodic, substrate-induced spatial modulation. This energy is minimized when the adlayer is rotated away from high-symmetry directions of the substrate and the model predicts the rotational epitaxy angle of the adlayer, which is a function of the adlayer lattice spacing. The following approximations are made in the NM model: (i) the interaction between adatoms is harmonic, (ii) the substrate is rigid, (iii) thermal effects are not important (the temperature is zero), and (iv) the substrate-induced spatial modulation is small. We have shown that approximation (iv) is correct, but have no direct evidence regarding the validity of the first three.

For Tl (Ref. 32) and Pb (Refs. 21, 22, 37, and 38) on Ag(111), the NM model predicts adlayer rotational epitaxy angles of $\simeq 5°$ and $\simeq 5.5°$, respectively, from the $\mathrm{Ag}[100]_h$ direction. These are within about a degree of what we measure. However, we do not observe any dependence of the rotation angle on lattice spacing,[21,22,32,37,38] in apparent disagreement with the NM model. One conceivable cause of the discrepancy is a small amount of impurity adsorption during the experiment,[32] since small quantities of adsorbed impurities have been shown to influence the rotation angle.[39] There are, however, several other possible explanations.[21,22,38] Keeping in mind the uncertainties due to this discrepancy and the unverified validity of the approximations used in the NM model, we will use this model to estimate the substrate potential-energy corrugation. We should emphasize that this is only an estimate.

With the above approximations, NM calculate $\mathbf{u}_\mathbf{G}$ as[4]

$$\mathbf{u}_\mathbf{G} = -i \sum_k \frac{[\boldsymbol{\varepsilon}_k(\mathbf{G})\cdot\mathbf{G}]}{M\omega_k^2(\mathbf{G})} V_\mathbf{G} \boldsymbol{\varepsilon}_k(\mathbf{G}) \ . \tag{9}$$

Here, M is the adatom mass, $\omega_k(\mathbf{G})$ and $\boldsymbol{\varepsilon}_k(\mathbf{G})$ are, respectively, the frequencies and polarization vectors of the phonons in the adlayer, and k is the phonon-mode label (longitudinal or transverse). The adsorbate-substrate interaction potential $V(\mathbf{r})$ has been decomposed into Fourier components[40]

$$V(\mathbf{r}) = \sum_\mathbf{G} V_\mathbf{G} \exp(i\mathbf{G}\cdot\mathbf{r}) \ . \tag{10}$$

In the long-wavelength limit, the relationship between u_G^l and V_G [Eq. (9)] becomes[4]

$$u_\mathrm{G}^l = \frac{V_\mathrm{G}}{GMc_l^2} \left[\frac{1}{1+z^2-2z\cos\Omega} + \frac{\eta z^2(\sin\Omega)^2}{(1+z^2-2z\cos\Omega)^2} \right] , \tag{11}$$

where $\eta = (c_l/c_t)^2 - 1$ and c_l and c_t are the adlayer longitudinal and transverse sound velocities, respectively. The rotational epitaxy angle Ω is the angle between the substrate and the adsorbate reciprocal lattice vectors, $\mathbf{G}$ and τ, respectively, and $z = \tau/G$. For Tl/Ag(111), $\mathbf{G}$ and τ are both lowest-order reciprocal-lattice vectors.

To calculate V_G from Eq. (11), it is necessary to determine the longitudinal and transverse sound velocities for the Tl monolayer. Although these have not been measured, we can estimate them using two models. In the simplest, we calculate the sound velocities of a very thin plate of Tl (Ref. 41) using the bulk, isotropic values of Young's modulus E and Poisson's ratio σ.[42,43] This yields $c_l = 1.4\times10^5$ cm/sec and $c_t = 4.8\times10^4$ cm/sec. An alternate approach models the monolayer as a very thin plate of Tl with the [001] direction normal to the plate, and this approach approximately accounts for elastic anisotropy by calculating[42] the in-plane values of E and σ from the bulk Tl elastic constants.[43] These elastic constants are used to estimate the sound velocities for the thin plate[41] with the results $c_l = 9.3\times10^4$ cm/sec and $c_t = 4.8\times10^4$ cm/sec. Neither model correctly treats elastic anisotropy and both ignore the fact that the force constants are different in a monolayer than in bulk. They are, however, adequate for our purpose. Using these sound velocities, we estimate that the first Fourier com-

ponent of the energy corrugation is V_G [$\mathbf{G}=(100)_h$]=2–3 meV (0.05–0.07 kcal/mol). We note that this is the corrugation energy for an atom *in a monolayer* when it is surrounded by other Tl adatoms. This energy is probably not the same as that for isolated adatoms due to the metallic (nonlocal) interactions between adatoms.

The estimated value of V_G [$\mathbf{G}=(100)_h$]=2–3 meV is only about 0.1% of the ~2 eV bond energy between Tl and Ag. (This bond energy is estimated as the sum of cohesive energy of bulk Tl plus the UPD shift.[25]) We are unaware of any theoretical predictions or measured values of V_G for metals adsorbed on other metals, and so, we cannot directly compare our value to others. However, it is reasonable to compare $3V_G$ to the activation energy for surface diffusion E_d, since these are both the energy required for an adatom to pass from the potential minimum to the potential saddle point. In general, for metals adsorbed in vacuum onto other metals, E_d is a few tenths of an eV or more,[44] significantly larger than $3V_G$. We speculate that this results because the diffusion measurements are made for isolated adatoms, while the corrugation energy we measure is for an adatom *within* a monolayer. Perhaps the metallic bonding between the adatoms within the monolayer reduces the energy corrugation caused by the substrate potential.

The best-fit center-to-center spacing between the Tl monolayer and the Ag substrate is 3.05±0.1 Å. This average separation is slightly smaller than the 3.16-Å spacing obtained by simply placing a rigid close-packed layer of Tl atoms (radius ≃1.72 Å) above a rigid close-packed layer of Ag atoms (radius ≃1.44 Å). Although the estimated accuracy of our determination makes it impossible to be certain that this difference is real, a smaller spacing is certainly reasonable, since most of the adatoms are not directly above Ag atoms but are instead near the hollow and bridge sites where they are closer to the Ag surface. Alternatively, the strong attraction between the adsorbate and substrate could cause a reduced spacing. Finally, the very large electric field present at the electrode-electrolyte interface may influence the attraction and thus the adlayer-substrate spacing. It will be interesting to see how the Ag-Tl spacing changes with applied potential.

As mentioned earlier, we assumed that the modulation normal to the surface is negligibly small. Fits to the ratio data in Fig. 4(c) with nonzero normal modulations did not result in improved fits compared to the fit with zero normal modulation. To determine this modulation, it will be necessary to obtain data to much larger Q_z.

The maxima and minima of the substrate-adsorbate interaction potential are easily calculated from the expression for $V(\mathbf{r})$ [Eq. (10)]. Since V_G is positive, the maxima occur at substrate positions $\{\mathbf{r}\}$ where $\mathbf{G}\cdot\mathbf{r}=2n\pi$ (n an integer); this is the set of sites directly above Ag atoms. The interaction energy minima are at the threefold-hollow sites, since these sites have $\mathbf{G}\cdot\mathbf{r}=(2n+1)\pi\pm\pi/3$ and minimize Eq. (10). It is not surprising that the threefold-hollow sites are the minimum energy sites for Tl on Ag(111), because at these sites the adatoms have maximum coordination. Indeed, in the vacuum-deposition studies of Tl on Ag(111), a low-coverage $(\sqrt{3}\times\sqrt{3})R30°$ structure is observed and in the proposed model for this structure, all the adatoms occupy threefold-hollow sites.[45]

To construct a real-space picture of the modulated Tl monolayer, the transverse component of the spatial modulation, $u_G^t=\mathbf{u}_G-u_G^l(\mathbf{G}/G)=\mathbf{u}_G\cdot(\hat{\mathbf{z}}\times\mathbf{G})/|\mathbf{G}|$, must be determined. Since x-ray scattering measures $\mathbf{G}\cdot\mathbf{u}$, we cannot directly measure this transverse modulation. However, by using the NM expression for $\mathbf{u}_G$ [Eq.

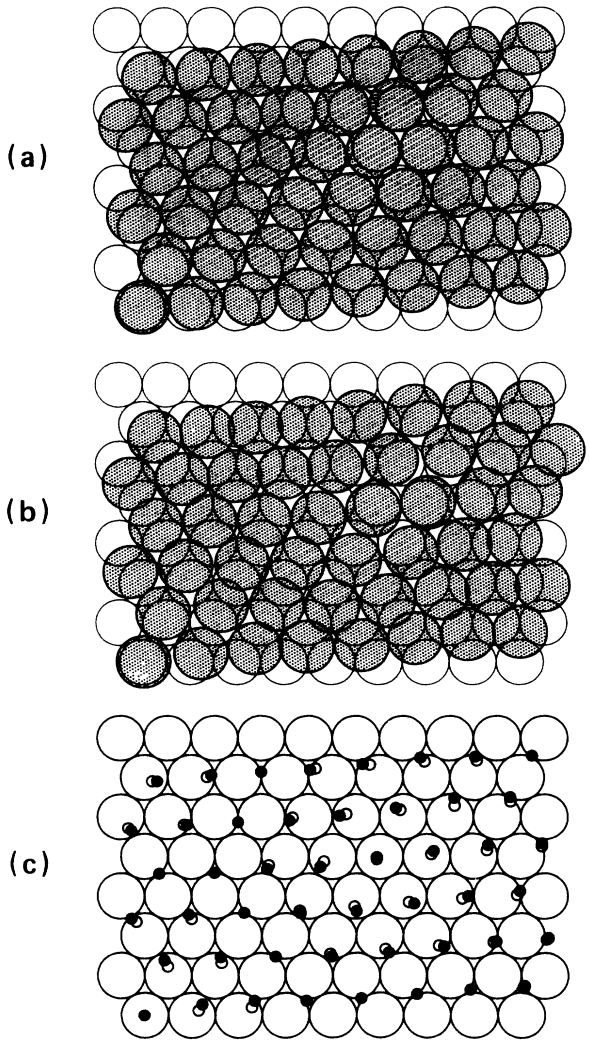

FIG. 5. Schematic real-space representation of one domain of monolayer Tl on Ag(111). The rotation angle between the Ag and Tl lattices is $\Omega=4.5°$ and the average near-neighbor spacing of the Tl monolayer is 3.34 Å (Ref. 32). The large open circles represent atoms in the Ag(111) surface and the shaded circles represent the Tl atoms; the lower leftmost adatom is arbitrarily positioned above an Ag atom. (a) The (hypothetical) unmodulated structure. (b) The modulated monolayer. The adatoms positions are calculated using Eq. (1). (c) A comparison between the modulated and unmodulated monolayers. The small solid (open) circles represent the adatoms positions in the modulated (unmodulated) adlayer. The adatom shift $\mathbf{u}_j$ is the difference between the two.

(9)] and our estimate for V_G, the transverse modulation is estimated as $u_G^l = 0.022$ Å, which is slightly smaller than u_G^l.

Figure 5 shows several schematic representations of the real-space structure of one domain of Tl on Ag(111). For comparative purposes, the hypothetical *unmodulated* adlayer is shown in Fig. 5(a). The open circles represent atoms of the Ag(111) surface and have a diameter proportional to their nearest-neighbor spacing (2.89 Å). The shaded circles represent the Tl adatoms and have a diameter proportional to 3.34 Å, which is their average nearest-neighbor spacing.[32] Figure 5(b) shows the positions of the adatoms in the modulated monolayer calculated using Eq. (1), the measured u_G^l and the estimated u_G^l. A comparison of Figs. 5(a) and 5(b) shows that the hypothetical, unmodulated adlayer adequately represents the average structure, but of course, ignores the subtle local structure. The local density increases and decreases are readily apparent in Fig. 5(b) as "overlapping" adatoms and "empty spaces" between adatoms, respectively. These density changes increase the adlayer elastic energy, but the decrease in the adsorbate-substrate energy due to the modulation more than compensates for this increase. This is illustrated in Fig. 5(c), which shows the adatom shifts $\mathbf{u}_j$. The small solid (open) circles represent the adatoms positions in the modulated (unmodulated) adlayer; $\mathbf{u}_j$ is the difference between the two. This figure shows a clear tendency for the adatoms to shift toward the minimum energy sites: the threefold hollows. The shifts are largest midway between the minimum energy sites and the maximum energy (on-top) sites, where the gradient of the adsorbate-substrate energy is largest.

Our method of measuring the interference between the substrate scattering and the scattering caused by the spatial modulation of the incommensurate adlayer is more sensitive to the modulation than measurements of the "satellite" diffraction [see Sec. II and Eq. (3)] caused by the modulation. This is because the interference depends on the product of A_m and A_s, which is linear in $\mathbf{u}_G$, while the satellite intensity depends on $(A_m)^2$, which is quadratic in $\mathbf{u}_G$ and consequently much smaller. Thus, the satellite scattering has only been observed when the substrate-induced modulation is strong and $\mathbf{u}_G$ is large.[9] Indeed, in earlier measurements of UPD Pb on Ag(111), we could not observe any satellite diffraction peaks (the satellite intensity was less than 3% of the main Pb peak).[46] If $\mathbf{u}_G$ [$\mathbf{G}=[100]_h$] for Pb on Ag(111) is similar to that for Tl on Ag(111), then the satellite peak intensity would only be about 0.6% of the main peak, and we would not have been able to observe it previously.[46] For Tl, this calculated satellite intensity is only 100 counts per second (cps), which is small compared to the background scattering rate of about 2000 cps. In addition, by measuring the satellites, it is not possible to determine directly the relative phase of the modulation scattering, since $|\mathbf{G}\cdot\mathbf{u}_G|^2$ is measured. In contrast, by measuring the interference between the adlayer and substrate scattering, this phase is readily determined.

It is interesting to compare our results with those of Reiter and Moss, who treated the x-ray scattering from a 2D *liquid* modulated by a periodic host substrate.[6] They found that the 2D modulated liquid contributes scattering intensity at the substrate diffraction peaks, and that from this contribution, the Fourier components of the surface energy corrugation V_G can be determined. Together with their co-workers, they have determined the Fourier components for Rb (Ref. 7) and K (Ref. 8) intercalated graphite. For both a 2D liquid and a 2D solid, the contribution to the substrate scattering has the same origin: the periodic spatial modulation induced by the substrate potential. However, the contribution to the substrate scattering in these two situations is different, because the elastic response of a solid to the substrate potential is different from that of a liquid. A solid will support shear but a liquid will not. Consequently, the scattering amplitudes depend on different physical properties of the adsorbed layer.

VI. SUMMARY AND CONCLUSIONS

By conducting *in situ* measurements of the intensities of crystal truncation rods from Ag(111) substrates both with and without a monolayer of electrochemically adsorbed Tl, we have determined the longitudinal (i.e., along $\mathbf{G}$) component of the first Fourier coefficient of the substrate-induced modulation of the incommensurate Tl monolayer (0.03 Å). The observed changes in the x-ray scattering arise because the spatial modulation induced by the substrate potential has wave vectors commensurate with the substrate periodicity. From scans made along the truncation rods, the spacing of the Tl monolayer above the Ag surface was also determined (3.05 Å). The first Fourier component of the surface potential-energy corrugation (2–3 meV = 0.05–0.07 kcal/mol) was estimated using the NM model[3,4] and estimates of the elastic susceptibility of the Tl monolayer. Because the phase of the monolayer scattering amplitude (relative to the substrate) could be determined, the sign of this Fourier component of the surface energy corrugation was determined. This identified the threefold-hollow sites as the lowest-energy sites on the surface. The data were analyzed by taking the ratio of the truncation-rod intensities with and without the monolayer adsorbed. This was very important, since the geometrical scattering corrections cancel out of the ratio and the ratio is considerably more accurate than the corrected intensities. The truncation-rod scans of the bare surface show that the immersed Ag surface is very smooth (a rms roughness of 0.7 Å).

These results demonstrate for the first time that surface x-ray scattering measurements of the *substrate* diffraction can be used to probe the substrate-induced modulation of *incommensurate* adlayers. Similar measurements will provide important structural information on many other systems, such as the substrate-induced modulation in thin epitaxial layers, other incommensurate adlayers, and the reconstructed top layers of some single crystals, such as Au(111) and Au(100).[47]

ACKNOWLEDGMENTS

We thank Jean Jordan-Sweet and Brian Stephenson for their assistance with beam line X20A and Ian Robinson for lending us his Soller slits. This work was partially supported by the Office of Naval Research. It was performed at the National Synchrotron Light Source (NSLS) at Brookhaven National Laboratory (Upton, NY), which is supported by the U. S. Department of Energy (DOE), Division of Material Sciences and Division of Chemical Sciences (DOE Contract No. DE-ACO2-76CH00016).

[1]F. C. Frank and J. H. van der Merwe, Proc. R. Soc. London Ser. A **198**, 205 (1949); **198**, 216 (1949).

[2]F. C. Frank and J. H. van der Merwe, Proc. R. Soc. London Ser. A **200**, 125 (1949); **198**, 261 (1949).

[3]A. D. Novaco and J. P. McTague, Phys. Rev. Lett. **38**, 1286 (1977).

[4]J. P. McTague and A. D. Novaco, Phys. Rev. B **19**, 5299 (1979).

[5]R. J. Birgeneau and P. M. Horn, Science **232**, 329 (1986).

[6]G. Reiter and S. C. Moss, Phys. Rev. B **33**, 7209 (1986).

[7]S. C. Moss, G. Reiter, J. L. Robertson, C. Thompson, J. D. Fan, and K. Oshima, Phys. Rev. Lett. **57**, 3191 (1986).

[8]X. B. Kan, J. L. Robertson, S. C. Moss, K. Ohshima, and C. J. Sparks, Phys. Rev. B **39**, 10 627 (1989).

[9]P. W. Stephens, P. A. Heiney, R. J. Birgeneau, P. M. Horn, D. E. Moncton, and G. S. Brown, Phys. Rev. B **29**, 3512 (1984).

[10]J. Villain and M. B. Gordon, Surf. Sci. **125**, 1 (1983).

[11]J. M. Cowley, J. B. Cohen, M. B. Salamon, and B. J. Wuensch, in *Modulated Structures—1979 (Kailua Kona, Hawaii)*, Proceedings of the International Conference on Modulated Structures, AIP Conf. Proc. No. 53, edited by J. M. Cowley, J. B. Cohen, M. B. Salamon, and B. J. Wuensch (AIP, New York, 1979).

[12]R. Pynn, Nature (London) **281**, 433 (1979).

[13]P. Bak, Rep. Prog. Phys. **45**, 587 (1982), and references therein.

[14]I. K. Robinson, Phys. Rev. B **33**, 3830 (1986).

[15]A. M. Afanas'ev, P. A. Aleksandrov, S. S. Fanchenko, V. A. Chaplanov, and S. S. Yakimov, Acta Crystallogr. Sect. A **42**, 116 (1986).

[16]S. R. Andrews and R. A. Cowley, J. Phys. C **18**, 6427 (1985).

[17]I. K. Robinson, W. K. Waskiewicz, R. T. Tung, and J. Bohr, Phys. Rev. Lett. **57**, 2714 (1986).

[18]R. Feidenhans'l, Surf. Sci. Rep. **10**, 105 (1989).

[19]This assumes that the substrate is rigid. Our analysis indicates this is valid, since there is no change in the substrate roughness on adsorption of the Tl.

[20]S. G. J. Mochrie, Phys. Rev. Lett. **59**, 304 (1987).

[21]M. G. Samant, M. F. Toney, G. L. Borges, L. Blum, and O. R. Melroy, Surf. Sci. **193**, L29 (1988).

[22]M. G. Samant, M. F. Toney, G. L. Borges, L. Blum, and O. R. Melroy, J. Phys. Chem. **92**, 220 (1988).

[23]E. D. Specht, A. Mak, C. Peters, M. Sutton, R. J. Birgeneau, K. L. D'Amico, D. E. Moncton, S. E. Nagler, and P. M. Horn, Z. Phys. B **69**, 347 (1987).

[24]W. R. Busing and H. A. Levy, Acta. Crystallogr. **22**, 457 (1967).

[25]D. Kolb, M. Przasnyski, and H. Gerischer, J. Electroanal. Chem. **54**, 25 (1974).

[26]D. M. Kolb, in *Advances in Electrochemistry and Electrochemical Engineering*, edited by H. Gerischer and C. W. Tobias (Wiley, New York, 1978), Vol. II, p. 125.

[27]D. M. Kolb, J. Vac. Sci. Technol. A **4**, 1294 (1986).

[28]H. Siegenthaler, K. Juttner, E. Schmidt, and W. J. Lorenz, Electrochim. Acta **23**, 1009 (1978).

[29]K. Juttner and H. Siegenthaler, Electrochim. Acta **23**, 971 (1978).

[30]W. J. Lorenz, H. D. Hermann, N. Wuthrich, and F. Hilbert, J. Electrochem. Soc. **121**, 1167 (1974).

[31]A. Bewick and B. Thomas, J. Electroanal. Chem. **65**, 911 (1975).

[32]M. F. Toney, J. G. Gordon, M. G. Samant, G. L. Borges, D. G. Wiesler, D. Yee, and L. B. Sorenson (unpublished).

[33]M. S. Altman, P. J. Estrup, and I. K. Robinson, Phys. Rev. B **38**, 5211 (1988).

[34]I. K. Robinson, Aust. J. Phys. **41**, 359 (1988).

[35]Although stacking faults can give rise to scattering intensity similar to that from CTR's, we cannot fit the data shown in Fig. 3 by assuming the film has stacking faults.

[36]J. M. MacLaren, J. B. Pendry, R. J. Rous, D. K. Saldin, G. A. Somorjai, M. A. Van Hove, and D. D. Vvedensky, *Surface Crystallographic Information Service: A Handbook of Surface Science* (Reidel, Dordrecht, 1987).

[37]M. F. Toney and O. R. Melroy, in *Synchrotron Radiation in Materials Research*, Vol. 143 of *Materials Research Society Symposia Proceedings*, edited by R. Clarke (MRS, Pittsburgh, 1989), p. 375.

[38]M. F. Toney and O. R. Melroy, in *In Situ Studies of Electrochemical Interfaces*, edited by H. D. Abruna (VCH Verlag Chemical, Berlin, 1990).

[39]K. Kern, P. Zeppenfeld, R. David, R. L. Palmer, and G. Comsa, Phys. Rev. Lett. **57**, 3187 (1986).

[40]W. A. Steele, *The Interaction of Gases with Solid Surfaces* (Pergamon, Oxford, 1974).

[41]L. D. Landau and E. M. Lifshitz, *Statistical Physics* (Addison-Wesley, Reading, 1969).

[42]J. F. Nye, *Physical Properties of Crystals* (Oxford University Press, London, 1957).

[43]G. Simmons and H. Wang, *Single Crystal Elastic Constants and Calculated Aggregate Properties: A Handbook* (MIT Press, Cambridge, MA, 1971).

[44]A. G. Naumovets and Yu. S. Vedula, Surf. Sci. Rep. **4**, 365 (1984).

[45]K. J. Rawlings, M. J. Gibson, and P. J. Dobson, J. Phys. D **11**, 2059 (1978).

[46]O. R. Melroy, M. F. Toney, G. L. Borges, M. G. Samant, J. B. Kortright, P. N. Ross, and L. Blum, Phys. Rev. B **38**, 10962 (1988).

[47]D. Gibbs, B. M. Ocko, D. M. Zehner, and S. G. J. Mochrie, Phys. Rev. B **38**, 7303 (1988).

[48]We have also fitted the data in Fig. 4(c) with Eq. (8) plus a Debye-Waller factor for the Tl monolayer (representing disorder perpendicular to the substrate). The use of this additional fitting parameter does not result in a significant improvement in the fit to the data; furthermore, it does not affect the best-fit values for the modulation u_G^l or the Ag-Tl spacing d.

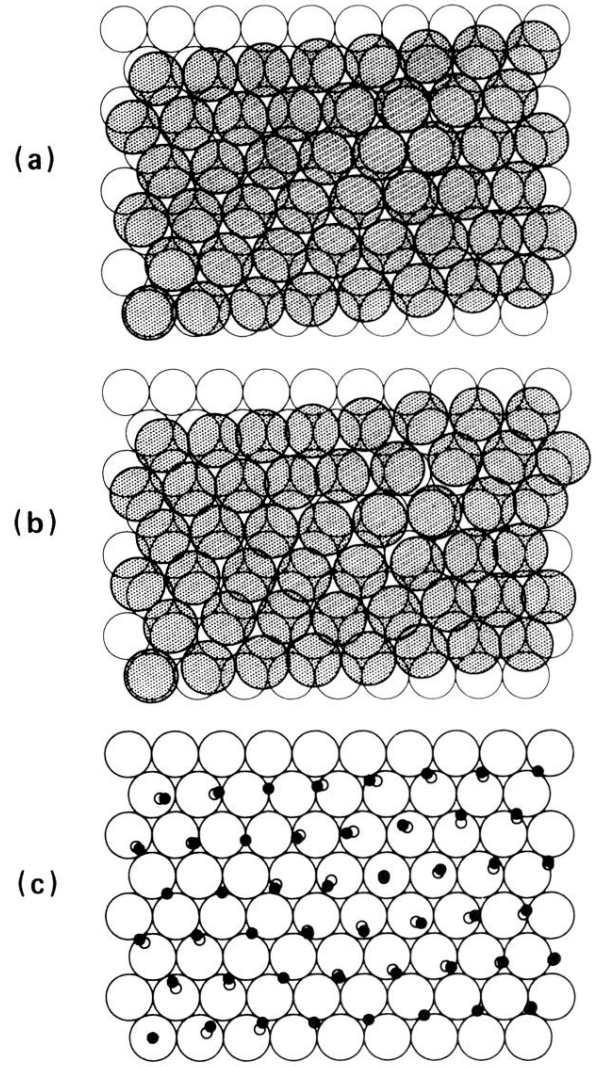

FIG. 5. Schematic real-space representation of one domain of monolayer Tl on Ag(111). The rotation angle between the Ag and Tl lattices is $\Omega = 4.5°$ and the average near-neighbor spacing of the Tl monolayer is 3.34 Å (Ref. 32). The large open circles represent atoms in the Ag(111) surface and the shaded circles represent the Tl atoms; the lower leftmost adatom is arbitrarily positioned above an Ag atom. (a) The (hypothetical) unmodulated structure. (b) The modulated monolayer. The adatoms positions are calculated using Eq. (1). (c) A comparison between the modulated and unmodulated monolayers. The small solid (open) circles represent the adatoms positions in the modulated (unmodulated) adlayer. The adatom shift $\mathbf{u}_j$ is the difference between the two.